Characteristics of second harmonic generation of Lamb waves in nonlinear elastic plates

Martin F. Müller and Jin-Yeon Kim
School of Civil and Environmental Engineering, Georgia Institute of Technology, Atlanta, Georgia 30332-0355

Jianmin Qu
G. W. Woodruff School of Mechanical Engineering, Georgia Institute of Technology, Atlanta, Georgia 30332-0405

Laurence J. Jacobs[a)]
School of Civil and Environmental Engineering and G. W. Woodruff School of Mechanical Engineering, Georgia Institute of Technology, Atlanta, Georgia 30332-0360

(Received 1 October 2009; revised 30 December 2009; accepted 30 December 2009)

This paper investigates the characteristics of the second harmonic generation of Lamb waves in a plate with quadratic nonlinearity. Analytical asymptotic solutions to Lamb waves are first obtained through the use of a perturbation method. Then, based on a careful analysis of these asymptotic solutions, it is shown that the cross-modal generation of a symmetric second harmonic mode by an antisymmetric primary mode is possible. These solutions also demonstrate that modes showing internal resonance—nonzero power flux to the second harmonic mode, plus phase velocity matching—are most useful for measurements. In addition, when using finite wave packets, which is the case in most experimental measurements, group velocity matching is required for a cumulative increase in the second harmonic amplitude with propagation distance. Finally, five mode types (which are independent of material properties) that satisfy all three requirements for this cumulative increase in second harmonic amplitude—nonzero power flux, plus phase and group velocity matching—are identified. These results are important for the development of an experimental procedure to measure material nonlinearity with Lamb waves.
 [DOI: 10.1121/1.3294714]

PACS number(s): 43.25.Dc, 43.20.Mv, 43.35.Cg [YHB] Pages: 2141–2152

I. INTRODUCTION

Recent research has demonstrated that nonlinear ultrasonic waves can be used to detect fatigue damage in its early stages.[1–4] This second harmonic generation describes a nonlinear acoustic effect where components are generated at twice the frequency of the excitation wave. These second harmonic acoustic components can be directly attributed to the nonlinear elastic properties of a material. As opposed to its linear elastic properties, these nonlinear elastic properties are much more sensitive to changes in the microstructure, such as those caused by fatigue damage. Experimental measurements of these second harmonic components[1–4] potentially enable the direct characterization of the nonlinear elastic properties and the associated damage state of a material.

The objective of this research is to determine the conditions for the second harmonic generation of Lamb waves in a plate with quadratic nonlinearity. Following the solution to this problem derived by de Lima and Hamilton,[5] analytical asymptotic solutions to Lamb waves are first obtained through the use of a perturbation method. Then, based on a careful analysis of these asymptotic solutions, it is shown that the cross-modal generation of a symmetric second harmonic mode by an antisymmetric primary mode is possible. This clarifies contradictory statements between de Lima and Hamilton,[5] Deng,[6] and Srivastava and di Scalea.[7] These solutions also demonstrate that modes showing internal resonance—nonzero power flux to the second harmonic mode, plus phase velocity matching—are most useful for measurements. In addition, when using finite wave packets, which is the case in most experimental measurements, group velocity matching is required for a cumulative increase in the second harmonic amplitude with propagation distance. Note that phase velocity matching requires that the phase velocities for the excitation mode at frequency ω and for the second harmonic mode at the double frequency, 2ω, be the same. Group velocity matching requires the same, but for the group velocity.

Finally, this paper identifies five mode types (which are independent of material properties) that satisfy all three requirements for this cumulative increase in second harmonic amplitude—nonzero power flux, plus phase and group velocity matching. The identification of these mode combinations is critical for the development of an experimental procedure to measure material nonlinearity with Lamb waves, which is important for material characterization and nondestructive evaluation (NDE) applications.

[a)]Author to whom correspondence should be addressed. Electronic mail: laurence.jacobs@coe.gatech.edu

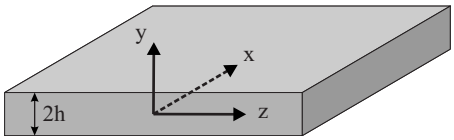

FIG. 1. Coordinate system of the infinite plate.

II. SECOND HARMONIC GENERATION

Consider an elastic, homogeneous, isotropic, infinite plate with quadratic nonlinearity. Guided Lamb waves propagate in the positive z-direction of this $2h$ thick plate, while the upper and lower surfaces at $y=\pm h$ are assumed to be stress free, as seen in Fig. 1.

Following the solution derived by de Lima and Hamilton,[5] consider a perturbation approach that expresses the overall solution of the displacement field as the sum of a primary wave $\boldsymbol{u}^{(1)}$, which is associated with the wave launched into the plate at frequency ω, and a secondary wave $\boldsymbol{u}^{(2)}$, which arises at twice the primary frequency, 2ω, and is the second harmonic wave generated by the quadratic nonlinearities in the plate, or

$$\boldsymbol{u}=\boldsymbol{u}^{(1)}+\boldsymbol{u}^{(2)}. \tag{1}$$

The perturbation condition,

$$|\boldsymbol{u}^{(2)}| \ll |\boldsymbol{u}^{(1)}|, \tag{2}$$

states that the nonlinear effect of second harmonic generation is very small compared to the primary wave. This method reduces the nonlinear boundary value problem to two linear boundary value problems: a homogeneous one for the primary wave and an inhomogeneous one for the secondary wave, which is forced by the primary wave.

The solution for the primary wave is given by linear Lamb mode theory.[8,9] Ignoring shear horizontal (SH) modes, the mode solution assumes the form

$$\boldsymbol{u}(y,z,t)=\tilde{\boldsymbol{u}}(y)e^{i(\kappa z-\omega t)}, \tag{3}$$

where the mode shape $\tilde{\boldsymbol{u}}(y)$ propagates harmonically in the z-direction. The Lamb mode $\tilde{\boldsymbol{u}}(y)$ can be either symmetric or antisymmetric, which is specified by the y-symmetry of the in-plane component $\tilde{u}_z(y)$. That is, for a symmetric (antisymmetric) Lamb mode, the in-plane component $\tilde{u}_z(y)$ is a symmetric (antisymmetric) function in y, while the out-of-plane component $\tilde{u}_y(y)$ is an antisymmetric (symmetric) function in y.

For symmetric Lamb modes, one obtains

$$\tilde{u}_y=i\frac{D}{h}\left(-\frac{(\bar{\kappa}^2-\bar{\beta}^2)\sin\bar{\beta}}{2\bar{\kappa}\sin\bar{\alpha}}\sin\left(\frac{\bar{\alpha}y}{h}\right)+\bar{\kappa}\sin\left(\frac{\bar{\beta}y}{h}\right)\right), \tag{4a}$$

$$\tilde{u}_z=-\frac{D}{h}\left(\frac{(\bar{\kappa}^2-\bar{\beta}^2)\sin\bar{\beta}}{2\bar{\alpha}\sin\bar{\alpha}}\cos\left(\frac{\bar{\alpha}y}{h}\right)+\bar{\beta}\cos\left(\frac{\bar{\beta}y}{h}\right)\right), \tag{4b}$$

where $\bar{\kappa}=\kappa h$ is the normalized Lamb wave number and $\bar{\omega}=\omega h$. Moreover,

$$\bar{\alpha}=\sqrt{(\bar{\omega}/c_L)^2-\bar{\kappa}^2},\quad \bar{\beta}=\sqrt{(\bar{\omega}/c_T)^2-\bar{\kappa}^2}, \tag{5}$$

where c_L is the longitudinal wave speed and c_T the shear wave speed in an unbounded medium. The complex coefficient D determines the amplitude of the mode and depends on the actual excitation of the mode. For antisymmetric Lamb modes, the solution is

$$\tilde{u}_y=i\frac{C}{h}\left(-\frac{(\bar{\kappa}^2-\bar{\beta}^2)\cos\bar{\beta}}{2\bar{\kappa}\cos\bar{\alpha}}\cos\left(\frac{\bar{\alpha}y}{h}\right)+\bar{\kappa}\cos\left(\frac{\bar{\beta}y}{h}\right)\right), \tag{6a}$$

$$\tilde{u}_z=\frac{C}{h}\left(\frac{(\bar{\kappa}^2-\bar{\beta}^2)\cos\bar{\beta}}{2\bar{\alpha}\cos\bar{\alpha}}\sin\left(\frac{\bar{\alpha}y}{h}\right)+\bar{\beta}\sin\left(\frac{\bar{\beta}y}{h}\right)\right), \tag{6b}$$

with the complex amplitude C. An important feature of Lamb modes is given by the dispersion relations between frequency and wave number, which allows for only modes with certain combinations of frequencies and wave numbers to propagate.

For the secondary boundary value problem, de Lima and Hamilton[5] employed a modal expansion technique. The secondary solution is written as

$$\boldsymbol{u}^{(2)}(y,z,t)=\sum_{n=1}^{N}A_n(z)\tilde{\boldsymbol{u}}_n(y)e^{-2i\omega t}, \tag{7}$$

which displays the sum of the N propagating linear modes at twice the primary frequency, 2ω, weighted by the respective amplitude coefficient $A_n(z)$ for each mode n in the expansion. This means that $A_n(z)$ determines how strong a certain secondary mode in the expansion is excited. Some manipulations, including a reciprocity relation and the orthogonality condition for linear modes, lead to an ordinary differential equation for $A_n(z)$, whose solution is given by

$$A_n(z)=\frac{f_n^{\mathrm{vol}}+f_n^{\mathrm{surf}}}{4\mathcal{P}_{nn}}\begin{cases}\dfrac{i}{\kappa_n^*-2\kappa}(e^{2i\kappa z}-e^{i\kappa_n^* z}) & \text{if } \kappa_n^*\neq 2\kappa\\ ze^{2i\kappa z} & \text{if } \kappa_n^*=2\kappa\end{cases}, \tag{8}$$

where κ is the Lamb wave number of the primary mode, κ_n is the Lamb wave number of the nth secondary mode in the expansion, the superscript " *" denotes the complex conjugate, and

$$\mathcal{P}_{nn}=-\frac{1}{2}\Re e\int_{-h}^{h}\tilde{\boldsymbol{v}}_n^*\cdot\tilde{\boldsymbol{\sigma}}_n\cdot\boldsymbol{n}_z dy \tag{9}$$

is the power carried by the nth secondary mode. $\boldsymbol{n}_z$ is the unit normal vector in z, $\tilde{\boldsymbol{v}}$ is the particle velocity, and $\tilde{\boldsymbol{\sigma}}$ is the linear stress tensor. It is seen that $A_n(z)$ is proportional to the sum of the terms

$$f_n^{\mathrm{vol}}=\int_{-h}^{h}\tilde{\boldsymbol{v}}_n^*\cdot\tilde{\boldsymbol{f}}^{2\omega}dy, \tag{10a}$$

$$f_n^{\text{surf}} = -\boldsymbol{n}_y \cdot \bar{\boldsymbol{S}}^{2\omega} \cdot \tilde{\boldsymbol{v}}_n^* \big|_{-h}^{h}, \tag{10b}$$

where $\boldsymbol{n}_y$ is the unit normal vector in the y-direction. f_n^{vol} and f_n^{surf} are interpreted physically as the power fluxes from the primary wave to the nth secondary mode due to material nonlinearities via volume body forces and surface tractions, respectively. This means that the stronger the power flux from the primary to the nth secondary mode, the stronger the secondary mode is excited. The power flux is caused by the body force $\bar{\boldsymbol{f}}^{2\omega}$ and surface tractions due to the stress tensor $\bar{\boldsymbol{S}}^{2\omega}$. These terms represent the complex 2ω-harmonic amplitude of the real quantities $\bar{\boldsymbol{f}}$ and $\bar{\boldsymbol{S}}$, which are given as

$$\begin{aligned}\bar{S}_{ij} = {} & \bar{B}\frac{\partial u_k}{\partial a_k}\frac{\partial u_i}{\partial a_j} + \frac{\bar{A}}{4}\frac{\partial u_i}{\partial a_k}\frac{\partial u_k}{\partial a_j} + (\lambda + \bar{B})\frac{\partial u_k}{\partial a_k}\frac{\partial u_j}{\partial a_i} + \left(\mu + \frac{\bar{A}}{4}\right) \\ & \times\left(\frac{\partial u_j}{\partial a_k}\frac{\partial u_i}{\partial a_k} + \frac{\partial u_k}{\partial a_j}\frac{\partial u_k}{\partial a_i} + \frac{\partial u_j}{\partial a_k}\frac{\partial u_k}{\partial a_i}\right) + \left(\frac{\lambda}{2}\frac{\partial u_k}{\partial a_l}\frac{\partial u_k}{\partial a_l}\right. \\ & \left. + \bar{C}\frac{\partial u_k}{\partial a_k}\frac{\partial u_l}{\partial a_l}\right)\delta_{ij} + \frac{\bar{B}}{2}\left(\frac{\partial u_k}{\partial a_l}\frac{\partial u_k}{\partial a_l} + \frac{\partial u_k}{\partial a_l}\frac{\partial u_l}{\partial a_k}\right)\delta_{ij}\end{aligned} \tag{11a}$$

in index notation, and

$$\bar{\boldsymbol{f}} = \nabla \cdot \bar{\boldsymbol{S}}. \tag{11b}$$

The quantities in Eq. (11a) are the real primary displacement field u_i, Lamé's constant λ, the shear modulus μ, the third-order elastic material constants[10] $\bar{A}$, $\bar{B}$, and $\bar{C}$, and the coordinates in the reference configuration $(a_1, a_2, a_3) = (x, y, z)$. Equation (11) is obtained by the perturbation of the nonlinear boundary value problem, when keeping up to quadratic terms of displacements in the constitutive relation.

III. SYMMETRY PROPERTIES

Based on the modal solution presented above, both de Lima and Hamilton[5] and Deng[6] concluded contradictory symmetry properties of the second harmonic wave. de Lima and Hamilton stated that a primary mode can generate a secondary mode only of the same symmetry, e.g., an antisymmetric primary mode can excite an antisymmetric, but not a symmetric second harmonic mode, and vice versa. In contrast, Deng stated that the second harmonic wave must be purely symmetric, thus contradicting de Lima and Hamilton. Note that Deng did not conclude explicitly that a symmetric secondary mode can be generated by an antisymmetric primary mode.

This section clarifies this symmetry issue by the use of the modal solution presented in Sec. II employing generic y-symmetric functions, similar to Srivastava and di Scalea.[7] Equations (7) and (8) show that a secondary mode n can be excited only if the power flux from the primary to the secondary mode is nonzero, i.e., if $f_n^{\text{vol}} + f_n^{\text{surf}} \neq 0$. In general, the computations of f_n^{vol} and f_n^{surf} are very lengthy. Conclusions on symmetries can be achieved, however, by utilizing simple symmetry properties of functions.

In preparation for demonstrating the symmetry properties of the forcing terms $\bar{\boldsymbol{f}}$ and $\bar{\boldsymbol{S}}$, the expression for $\bar{\boldsymbol{S}}$ in Eq. (11a) is expanded for the two dimensions y and z, since the x-component of the displacement field for Lamb modes is zero when plane strain is assumed, i.e., $\partial/\partial x = 0$. This result is shown in the Appendix.

Now, let the primary mode be a symmetric Lamb mode whose displacement field is given in Eq. (4). In order to investigate symmetries along the y-axis, the following notation is introduced: $\mathcal{S}(y)$ is a generic, unspecified element of the set of symmetric functions in y, while $\mathcal{A}(y)$ is a generic, unspecified element of the set of antisymmetric functions in y. As discussed earlier, $u_y = \mathcal{A}(y)$ and $u_z = \mathcal{S}(y)$ hold for a symmetric mode. It is also seen that a derivative of u_i with respect to y changes the type of symmetry in y, while a derivative with respect to z does not change the type of symmetry in y. Moreover, the following rules are known:

(1) $\mathcal{S}(y) \cdot \mathcal{S}(y) = \mathcal{S}(y)$ and $\mathcal{A}(y) \cdot \mathcal{A}(y) = \mathcal{S}(y)$.
(2) $\mathcal{A}(y) \cdot \mathcal{S}(y) = \mathcal{A}(y)$ and $\mathcal{S}(y) \cdot \mathcal{A}(y) = \mathcal{A}(y)$.
(3) $\mathcal{S}(y) + \mathcal{S}(y) = \mathcal{S}(y)$ and $\mathcal{A}(y) + \mathcal{A}(y) = \mathcal{A}(y)$.

Using these results, the symmetry of the first term of Eq. (A1) is calculated as

$$\frac{\partial u_y}{\partial y}\frac{\partial u_y}{\partial y} = \mathcal{S}(y) \cdot \mathcal{S}(y) = \mathcal{S}(y).$$

In the same way, it is easily shown that all the terms on the diagonal of $\bar{\boldsymbol{S}}$ are $\mathcal{S}(y)$, while all the off-diagonal terms are $\mathcal{A}(y)$; hence

$$\bar{\boldsymbol{S}}_{\text{sym}} = \begin{pmatrix} \mathcal{S}(y) & \mathcal{A}(y) \\ \mathcal{A}(y) & \mathcal{S}(y) \end{pmatrix}. \tag{12a}$$

Furthermore, by Eq. (11b),

$$\bar{\boldsymbol{f}}_{\text{sym}} = \begin{pmatrix} \frac{\partial}{\partial y} & \frac{\partial}{\partial z} \end{pmatrix} \cdot \begin{pmatrix} \mathcal{S}(y) & \mathcal{A}(y) \\ \mathcal{A}(y) & \mathcal{S}(y) \end{pmatrix} = \begin{pmatrix} \mathcal{A}(y) \\ \mathcal{S}(y) \end{pmatrix}, \tag{12b}$$

where the subscript stands for the type of symmetry of the primary mode.

If the primary mode is antisymmetric, Eq. (6) shows that $u_y = \mathcal{S}(y)$ and $u_z = \mathcal{A}(y)$. Application to the same exemplary term above

$$\frac{\partial u_y}{\partial y}\frac{\partial u_y}{\partial y} = \mathcal{A}(y) \cdot \mathcal{A}(y) = \mathcal{S}(y)$$

yields the same result for that of a symmetric primary mode. This is explained by the fact that products of displacements are involved—even though each single term changes its symmetry in y, as compared to the analysis of a symmetric primary mode, the product rules lead back to the same result. Hence,

$$\bar{\boldsymbol{S}} = \begin{pmatrix} \mathcal{S}(y) & \mathcal{A}(y) \\ \mathcal{A}(y) & \mathcal{S}(y) \end{pmatrix}, \tag{13a}$$

and

$$\bar{\boldsymbol{f}} = \begin{pmatrix} \mathcal{A}(y) & \mathcal{S}(y) \end{pmatrix}^T, \tag{13b}$$

independent of the primary mode's symmetry. Since $\bar{\boldsymbol{f}}^{2\omega}$ and $\bar{\boldsymbol{S}}^{2\omega}$ are the complex harmonic amplitudes of $\bar{\boldsymbol{f}}$ and $\bar{\boldsymbol{S}}$, they show the same symmetry properties.

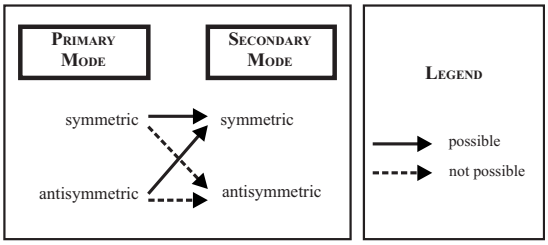

FIG. 2. Symmetry scheme of the second harmonic Lamb wave generation.

Recalling Eq. (10), the result for the power fluxes f_n^{vol} and f_n^{surf} depend on the symmetry properties of the secondary mode n. From $\tilde{\boldsymbol{v}}=i\omega\tilde{\boldsymbol{u}}$, one concludes

$$\tilde{\boldsymbol{v}}_{\mathrm{sym}}=\begin{pmatrix}\mathcal{A}(y) & \mathcal{S}(y)\end{pmatrix}^T \tag{14a}$$

for a symmetric mode, and

$$\tilde{\boldsymbol{v}}_{\mathrm{asym}}=\begin{pmatrix}\mathcal{S}(y) & \mathcal{A}(y)\end{pmatrix}^T \tag{14b}$$

for an antisymmetric mode. Finally, with $\mathbf{n}_y=(1,\ 0)$ and the secondary mode being symmetric, Eq. (10) becomes

$$f_n^{\mathrm{surf}}=\begin{pmatrix}1, & 0\end{pmatrix}\cdot\begin{pmatrix}\mathcal{S}(y) & \mathcal{A}(y)\\ \mathcal{A}(y) & \mathcal{S}(y)\end{pmatrix}\cdot\begin{pmatrix}\mathcal{A}(y)\\ \mathcal{S}(y)\end{pmatrix}\Bigg|_{y=-h}^{h}$$
$$=\mathcal{A}(y)\big|_{y=-h}^{h}\neq 0, \tag{15a}$$

$$f_n^{\mathrm{vol}}=\int_{y=-h}^{h}\begin{pmatrix}\mathcal{A}(y)\\ \mathcal{S}(y)\end{pmatrix}^T\cdot\begin{pmatrix}\mathcal{A}(y)\\ \mathcal{S}(y)\end{pmatrix}dy=\int_{y=-h}^{h}\mathcal{S}(y)dy\neq 0. \tag{15b}$$

It is noted that the inequality to zero holds in general, but there might be special frequencies and pairs of primary and secondary modes, for which at least one of these terms or their sum can be zero. Thus, if the secondary mode is symmetric, $A_n(z)\neq 0$ holds generally.

For the secondary mode being antisymmetric, one obtains

$$f_n^{\mathrm{surf}}=\begin{pmatrix}1, & 0\end{pmatrix}\cdot\begin{pmatrix}\mathcal{S}(y) & \mathcal{A}(y)\\ \mathcal{A}(y) & \mathcal{S}(y)\end{pmatrix}\cdot\begin{pmatrix}\mathcal{S}(y)\\ \mathcal{A}(y)\end{pmatrix}\Bigg|_{y=-h}^{h}$$
$$=\mathcal{S}(y)\big|_{y=-h}^{h}=0, \tag{16a}$$

$$f_n^{\mathrm{vol}}=\int_{y=-h}^{h}\begin{pmatrix}\mathcal{S}(y)\\ \mathcal{A}(y)\end{pmatrix}^T\cdot\begin{pmatrix}\mathcal{A}(y)\\ \mathcal{S}(y)\end{pmatrix}dy=\int_{y=-h}^{h}\mathcal{A}(y)dy=0, \tag{16b}$$

implying that $A_n(z)=0$ according to Eq. (8).

Summarizing these results, it is concluded that both a symmetric and an antisymmetric primary mode can excite a symmetric mode at twice the primary frequency. In contrast, neither a symmetric nor an antisymmetric primary mode can excite an antisymmetric mode at twice the primary frequency. Figure 2 displays this result graphically. Other authors[6,7,11] stated that the secondary wave is purely symmetric at the double frequency. However, they do not mention explicitly that the cross-modal excitation from an antisymmetric primary mode to a symmetric secondary mode is possible.

IV. INTERNAL RESONANCE

Recalling the modal solution in Sec. II, de Lima and Hamilton[5] observed that the amplitude coefficient $A_n(z)$ in Eq. (8) shows two fundamentally different behaviors depending on the relation between the wave numbers of the primary mode and the nth secondary mode. Noting the definition of the phase velocity

$$c_{\mathrm{ph}}=\frac{\omega}{k}, \tag{17}$$

the second case in Eq. (8) is referred to as phase velocity matching, since $\kappa^{(2\omega)}=2\kappa$ and $\omega^{(2\omega)}=2\omega$ imply that

$$c_{\mathrm{ph}}^{(2\omega)}=\frac{\omega^{(2\omega)}}{\kappa^{(2\omega)}}=\frac{\omega}{\kappa}=c_{\mathrm{ph}}, \tag{18}$$

where the superscript (2ω) denotes the terms associated with the second harmonic mode. Also note from Eq. (5) that for the case of phase velocity matching, $\bar{\alpha}^{(2\omega)}=2\bar{\alpha}$ and $\bar{\beta}^{(2\omega)}=2\bar{\beta}$.

If in addition to phase velocity matching, nonzero power flux from the primary to the secondary wave is assumed, the secondary mode shows internal resonance. In this case, the solution for the nth mode in the expansion takes the form

$$\boldsymbol{u}_n^{(2)}=\frac{f_n^{\mathrm{vol}}+f_n^{\mathrm{surf}}}{4\mathcal{P}_{nn}}z\tilde{\boldsymbol{u}}_n^{(2)}(y)\,e^{2i(\kappa z-\omega t)}. \tag{19}$$

The term internal resonance[5] is motivated by the linearly growing amplitude with propagation distance, z. This proportionality between the amplitude and the propagation distance suggests that the secondary mode can grow without any bounds. However, this behavior is prohibited by the perturbation condition of Eq. (2), which means that the perturbation solution is valid only up to a certain propagation distance.

de Lima and Hamilton[5] also mentioned that the nonresonant solution in Eq. (8), where $\kappa^{(2\omega)}\neq 2\kappa$, results in the sinusoidal behavior

$$\boldsymbol{u}_n^{(2)}=\frac{f_n^{\mathrm{vol}}+f_n^{\mathrm{surf}}}{2\mathcal{P}_{nn}\kappa_d}\sin\left(\frac{1}{2}\kappa_d z\right)\tilde{\boldsymbol{u}}_n^{(2)}(y)\,e^{i((1/2)(2\kappa+\kappa^{(2\omega)})z-2\omega t)}, \tag{20}$$

where $\kappa_d=\kappa^{(2\omega)}-2\kappa$ is interpreted as the deviance from exact phase velocity matching. In general, this nonresonant solution is not desirable, since displacements are bounded, and there are distances z where the amplitude is identically zero. However, a special case not mentioned in de Lima and Hamilton[5] is practically relevant; if κ_d is very small, the nonresonant solution approaches the resonant solution. In this case of approximate phase velocity matching, the second harmonic solution grows at an almost linear rate with propagation distance. Figure 3 shows the qualitative behavior of the amplitude depending on phase velocity matching.

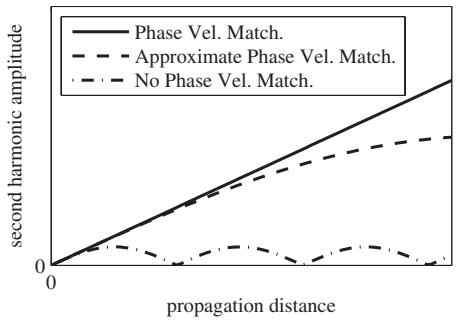

FIG. 3. Qualitative behavior of the second harmonic amplitude depending on phase velocity matching.

For material's characterization applications in NDE, exact or approximate internal resonance has several advantages. First, the growing amplitude results in large displacements after some propagation distance, improving the signal-to-noise ratio for measurements. In addition, other modes that are not in internal resonance may be disregarded as small when compared to the mode in resonance, after some distance, so that they do not interfere with the resonant mode under consideration.

V. GROUP VELOCITY MATCHING

Knowing that exact or approximate internal resonance is a desirable feature, finally, consider the additional importance of group velocity matching for practical measurements. In practice, the group velocity

$$c_g = \frac{d\omega}{d\kappa} = \frac{d\bar{\omega}}{d\bar{\kappa}} \tag{21}$$

plays an important role, since the group velocity—and not the phase velocity—is the propagation velocity of the energy of finite "wave packets" with similar frequencies. It follows that signals of different group velocities will shift relative to each other with propagation distance. Thus, if the primary and the secondary modes have different group velocities, the initial secondary mode generated at the beginning will separate locally from the primary mode, making the power flux from the primary to the initial secondary mode zero. This results in a bounded secondary wave whose amplitude does not show a linear increase with propagation distance. Therefore, for practical applications which employ finite wave packets, group velocity matching is required. Group velocity matching is defined as $c_g^{(2\omega)} = c_g$.

While it is commonly agreed that phase velocity matching is a necessary condition, the concept of group velocity matching is more controversial. Deng *et al.*,[12] for instance, did not believe that group velocity matching is a necessary condition, while Lee *et al.*[13] supported the argument given above. The analytical complexity to describe the influence of the group velocity on time-domain signals makes analytical arguments difficult to prove. The physical interpretation given above suggests group velocity matching at least as an adjuvant condition, if not necessary.

Two expressions of the group velocity in terms of the variables $\bar{\omega}$, $\bar{\kappa}$, and c_{ph} will be stated for future reference. Note that according to Eq. (17), only two of these variables are independent. First, the frequency equations from the linear elastic theory[8] for symmetric and for antisymmetric modes, respectively, are

$$\Phi_{\mathrm{sym}}(\bar{\omega},\bar{\kappa}) = \cos\bar{\alpha}\sin\bar{\beta}\,(\bar{\kappa}^2-\bar{\beta}^2)^2 + \sin\bar{\alpha}\cos\bar{\beta}\,4\bar{\alpha}\bar{\beta}\bar{\kappa}^2 = 0 \tag{22}$$

and

$$\Phi_{\mathrm{asym}}(\bar{\omega},\bar{\kappa}) = \sin\bar{\alpha}\cos\bar{\beta}\,(\bar{\kappa}^2-\bar{\beta}^2)^2 + \cos\bar{\alpha}\sin\bar{\beta}\,4\bar{\alpha}\bar{\beta}\bar{\kappa}^2 = 0, \tag{23}$$

representing implicit functions of $\bar{\omega}$ and $\bar{\kappa}$. Following Pilarski *et al.*,[14] if $\bar{\omega}$ is regarded as $\bar{\omega}=\bar{\omega}(\bar{\kappa})$, the group velocity is written as

$$c_{g,\mathrm{sym}} = -\frac{\partial\Phi_{\mathrm{sym}}/\partial\bar{\kappa}}{\partial\Phi_{\mathrm{sym}}/\partial\bar{\omega}} = \frac{N_{\mathrm{sym}}}{D_{\mathrm{sym}}} \tag{24}$$

and

$$c_{g,\mathrm{asym}} = -\frac{\partial\Phi_{\mathrm{asym}}/\partial\bar{\kappa}}{\partial\Phi_{\mathrm{asym}}/\partial\bar{\omega}} = \frac{N_{\mathrm{asym}}}{D_{\mathrm{asym}}}, \tag{25}$$

according to Eq. (21) and the rules of derivatives of implicit functions. By carrying out these derivatives, one obtains

$$\begin{aligned} N_{\mathrm{sym}} = {} & \cos\bar{\alpha}\cos\bar{\beta}\,[\bar{\alpha}\bar{\kappa}(\bar{\kappa}^2-\bar{\beta}^2)^2+4\bar{\alpha}\bar{\beta}^2\bar{\kappa}^3] \\ & -\sin\bar{\alpha}\sin\bar{\beta}\,[\bar{\beta}\bar{\kappa}(\bar{\kappa}^2-\bar{\beta}^2)^2+4\bar{\alpha}^2\bar{\beta}\bar{\kappa}^3] \\ & +\sin\bar{\alpha}\cos\bar{\beta}\,[4\bar{\beta}^2\bar{\kappa}^3+4\bar{\alpha}^2\bar{\kappa}^3-8\bar{\alpha}^2\bar{\beta}^2\bar{\kappa}] \\ & -\cos\bar{\alpha}\sin\bar{\beta}\,8\bar{\alpha}\bar{\beta}\bar{\kappa}(\bar{\kappa}^2-\bar{\beta}^2), \end{aligned} \tag{26a}$$

$$\begin{aligned} D_{\mathrm{sym}} = {} & \cos\bar{\alpha}\cos\bar{\beta}\left[\bar{\alpha}\frac{\bar{\omega}}{c_T^2}(\bar{\kappa}^2-\bar{\beta}^2)^2+4\bar{\alpha}\bar{\beta}^2\bar{\kappa}^2\frac{\bar{\omega}}{c_L^2}\right] \\ & -\sin\bar{\alpha}\sin\bar{\beta}\left[\bar{\beta}\frac{\bar{\omega}}{c_L^2}(\bar{\kappa}^2-\bar{\beta}^2)^2+4\bar{\alpha}^2\bar{\beta}\bar{\kappa}^2\frac{\bar{\omega}}{c_T^2}\right] \\ & +\sin\bar{\alpha}\cos\bar{\beta}\left[4\bar{\beta}^2\bar{\kappa}^2\frac{\bar{\omega}}{c_L^2}+4\bar{\alpha}^2\bar{\kappa}^2\frac{\bar{\omega}}{c_T^2}\right] \\ & -\cos\bar{\alpha}\sin\bar{\beta}\,4\bar{\alpha}\bar{\beta}\frac{\bar{\omega}}{c_T^2}(\bar{\kappa}^2-\bar{\beta}^2) \end{aligned} \tag{26b}$$

for symmetric modes, and

$$\begin{aligned} N_{\mathrm{asym}} = {} & \cos\bar{\alpha}\cos\bar{\beta}\,[\bar{\beta}\bar{\kappa}(\bar{\kappa}^2-\bar{\beta}^2)^2+4\bar{\alpha}^2\bar{\beta}\bar{\kappa}^3] \\ & -\sin\bar{\alpha}\sin\bar{\beta}\,[\bar{\alpha}\bar{\kappa}(\bar{\kappa}^2-\bar{\beta}^2)^2+4\bar{\alpha}\bar{\beta}^2\bar{\kappa}^3] \\ & -\sin\bar{\alpha}\cos\bar{\beta}\,8\bar{\alpha}\bar{\beta}\bar{\kappa}(\bar{\kappa}^2-\bar{\beta}^2) \\ & +\cos\bar{\alpha}\sin\bar{\beta}\,[4\bar{\beta}^2\bar{\kappa}^3+4\bar{\alpha}^2\bar{\kappa}^3-8\bar{\alpha}^2\bar{\beta}^2\bar{\kappa}], \end{aligned} \tag{27a}$$

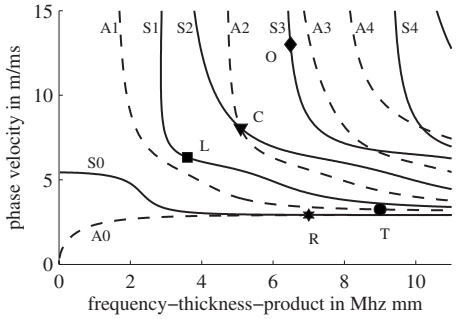

FIG. 4. Dispersion curves for an aluminum plate with matching mode pairs: C—crossing, L—symmetric modes at longitudinal phase velocity, O—cutoff frequency, T—nonzero order modes with a high wave number, and R—quasi-Rayleigh wave.

$$D_{\text{asym}} = \cos\bar{\alpha}\cos\bar{\beta}\left[\bar{\beta}\frac{\bar{\omega}}{c_L^2}(\bar{\kappa}^2-\bar{\beta}^2)^2+4\bar{\alpha}^2\bar{\beta}\bar{\kappa}^2\frac{\bar{\omega}}{c_T^2}\right] - \sin\bar{\alpha}\sin\bar{\beta}\left[\bar{\alpha}\frac{\bar{\omega}}{c_T^2}(\bar{\kappa}^2-\bar{\beta}^2)^2+4\bar{\alpha}\bar{\beta}^2\bar{\kappa}^2\frac{\bar{\omega}}{c_L^2}\right] - \sin\bar{\alpha}\cos\bar{\beta}\,4\bar{\alpha}\bar{\beta}\frac{\bar{\omega}}{c_T^2}(\bar{\kappa}^2-\bar{\beta}^2) + \cos\bar{\alpha}\sin\bar{\beta}\left[4\bar{\beta}^2\bar{\kappa}^2\frac{\bar{\omega}}{c_L^2}+4\bar{\alpha}^2\bar{\kappa}^2\frac{\bar{\omega}}{c_T^2}\right] \tag{27b}$$

for antisymmetric modes. It should be noted that both $\bar{\alpha}$ and $\bar{\beta}$ are functions of $\bar{\omega}$ and $\bar{\kappa}$. Rose[15] presented a description of the group velocity in terms of $\bar{\omega}$ and c_{ph}.

$$c_g = c_{\text{ph}}^2\left(c_{\text{ph}}-\bar{\omega}\frac{dc_{\text{ph}}}{d\bar{\omega}}\right)^{-1}. \tag{28}$$

VI. CHARACTERISTICS OF MATCHING MODE PAIRS

Finally, five mode types (which are independent of material properties) that satisfy all three requirements for a cumulative increase in second harmonic amplitude with propagation distance—nonzero power flux, plus phase and group velocity matching—are identified. Figure 4 shows an example for each type in the dispersion curves for an aluminum plate (c_L=6320 m/ms, c_T=3130 m/ms), featuring crossing points (C), symmetric modes at the longitudinal phase velocity (L), nonzero order modes near cutoff frequencies (O), nonzero order modes with a high wave number (T), and the fundamental modes $A0$ and $S0$ with a high wave number (quasi-Rayleigh wave) (R). Each matching pair is considered in detail to determine their usefulness for practical measurements, with an emphasis on conditions for specific frequencies and wave numbers, plus the amplitudes of surface displacements, particularly out-of-plane motion, which tends to be easier to experimentally measure.

A. Crossing points

A crossing point is defined as a $(\bar{\omega},\bar{\kappa})$-pair for which a symmetric and an antisymmetric mode cross in the dispersion curves. It turns out that this is possible in the region $c_{\text{ph}}>c_L$, where both $\bar{\alpha}$ and $\bar{\beta}$ are real and positive. Thus, at a crossing point, both Eqs. (22) and (23) need to be satisfied simultaneously. By subtraction of Eq. (22) from Eq. (23), one obtains

$$(\sin\bar{\alpha}\cos\bar{\beta}-\cos\bar{\alpha}\sin\bar{\beta})((\bar{\kappa}^2-\bar{\beta}^2)^2-4\bar{\alpha}\bar{\beta}\bar{\kappa}^2)=0. \tag{29}$$

Solving for the term $(\bar{\kappa}^2-\bar{\beta}^2)^2-4\bar{\alpha}\bar{\beta}\bar{\kappa}^2=0$ reduces to the Rayleigh wave speed c_R, which is not the solution sought, since $c_R<c_L$. Hence, from Eq. (29),

$$\sin\bar{\alpha}\cos\bar{\beta}-\cos\bar{\alpha}\sin\bar{\beta}=\sin(\bar{\alpha}-\bar{\beta})=0 \tag{30}$$

or

$$\bar{\alpha}-\bar{\beta}=n\pi,\quad n\in\mathbb{N} \tag{31}$$

is inferred. Substituting this condition into Eq. (22) yields

$$\cos\bar{\beta}\sin\bar{\beta}\,(\bar{\kappa}^2-\bar{\beta}^2)^2+\sin\bar{\beta}\cos\bar{\beta}\,4\bar{\alpha}\bar{\beta}\bar{\kappa}^2=0; \tag{32}$$

hence one concludes

$$\bar{\beta}=n\pi/2,\quad n\in\mathbb{N}^+. \tag{33}$$

Recalling Eq. (31), it is proved that at a crossing point, either case I

$$\bar{\beta}=n_\beta\pi,\quad \bar{\alpha}=n_\alpha\pi,\quad n_\beta,n_\alpha\in\mathbb{N}^+, \tag{34}$$

or case II

$$\bar{\beta}=\frac{(2n_\beta-1)\pi}{2},\quad \bar{\alpha}=\frac{(2n_\alpha-1)\pi}{2},\quad n_\beta,n_\alpha\in\mathbb{N}^+ \tag{35}$$

must hold. Note that $n_\beta>n_\alpha$ by the definition of $\bar{\alpha}$ and $\bar{\beta}$. Using Eq. (5), these conditions allow for the computation of the corresponding frequencies as

$$\bar{\omega}=\sqrt{\frac{n}{c_L^2-c_T^2}}c_Lc_T\pi, \tag{36}$$

where $n=n_\beta^2-n_\alpha^2$ for case I and $n=n_\beta(n_\beta-1)-n_\alpha(n_\alpha-1)$ for case II.

Assuming phase velocity matching, it is concluded for both cases that

$$\bar{\beta}^{(2\omega)}=\bar{n}_\beta\pi,\quad \bar{\alpha}^{(2\omega)}=\bar{n}_\alpha\pi,\quad \bar{n}_\beta,\bar{n}_\alpha\in\mathbb{N}^+, \tag{37}$$

at frequency $2\bar{\omega}$. For case I, both $\bar{n}_\beta$ and $\bar{n}_\alpha$ are even, and odd for case II. This fulfills Eq. (34) and it follows that $(\bar{\omega}^{(2\omega)},\bar{\kappa}^{(2\omega)})$ is a crossing point of case I, which matches phase velocity with the point $(\bar{\omega},\bar{\kappa})$. By the definition of a crossing point, it is obvious that there is phase velocity matching from the symmetric as well as from the antisymmetric mode to both the symmetric and antisymmetric modes at the double frequency.

For the group velocities, the results from Eqs. (24), (25), (26a), (26b), (27a), and (27b) are recalled. For case I, using Eq. (34), the group velocities are

$$c_{g,\text{sym}}^{\text{I}}=\frac{\bar{\kappa}(\bar{\kappa}^2-\bar{\beta}^2)^2+4\bar{\beta}^2\bar{\kappa}^3}{(\bar{\omega}/c_T^2)(\bar{\kappa}^2-\bar{\beta}^2)^2+4\bar{\beta}^2\bar{\kappa}^2(\bar{\omega}/c_L^2)}, \tag{38}$$

TABLE I. Phase velocity matching mode pairs at crossing points.

From mode at $\bar{\omega}$				To mode at $2\bar{\omega}$				
Sym.	Case	$\tilde{u}_y(h)$	$\tilde{u}_z(h)$	Sym.	Case	$\tilde{u}_y(h)$	$\tilde{u}_z(h)$	Group match.
Sym	I	0	$\neq 0$	Sym	I	0	$\neq 0$	Yes
Asym	II	0	$\neq 0$	Sym	I	0	$\neq 0$	Yes
Sym	II	$\neq 0$	0	Sym	I	0	$\neq 0$	No
Asym	I	$\neq 0$	0	Sym	I	0	$\neq 0$	No
Asym	I	$\neq 0$	0	Asym	I	$\neq 0$	0	Yes
Sym	II	$\neq 0$	0	Asym	I	$\neq 0$	0	Yes
Asym	II	0	$\neq 0$	Asym	I	$\neq 0$	0	No
Sym	I	0	$\neq 0$	Asym	I	$\neq 0$	0	No

$$c_{g,\mathrm{asym}}^{\mathrm{I}} = \frac{\bar{\kappa}(\bar{\kappa}^2 - \bar{\beta}^2)^2 + 4\bar{\alpha}^2\bar{\kappa}^3}{(\bar{\omega}/c_L^2)(\bar{\kappa}^2 - \bar{\beta}^2)^2 + 4\bar{\alpha}^2\bar{\kappa}^2(\bar{\omega}/c_T^2)}, \tag{39}$$

while for case II, using Eq. (35), one arrives at

$$c_{g,\mathrm{sym}}^{\mathrm{II}} = \frac{\bar{\kappa}(\bar{\kappa}^2 - \bar{\beta}^2)^2 + 4\bar{\alpha}^2\bar{\kappa}^3}{(\bar{\omega}/c_L^2)(\bar{\kappa}^2 - \bar{\beta}^2)^2 + 4\bar{\alpha}^2\bar{\kappa}^2(\bar{\omega}/c_T^2)}, \tag{40}$$

$$c_{g,\mathrm{asym}}^{\mathrm{II}} = \frac{\bar{\kappa}(\bar{\kappa}^2 - \bar{\beta}^2)^2 + 4\bar{\beta}^2\bar{\kappa}^3}{(\bar{\omega}/c_T^2)(\bar{\kappa}^2 - \bar{\beta}^2)^2 + 4\bar{\beta}^2\bar{\kappa}^2(\bar{\omega}/c_L^2)}. \tag{41}$$

Note that $c_{g,\mathrm{sym}}^{\mathrm{I}} = c_{g,\mathrm{asym}}^{\mathrm{II}}$ and $c_{g,\mathrm{sym}}^{\mathrm{II}} = c_{g,\mathrm{asym}}^{\mathrm{I}}$.

Regarding the crossing point at the double frequency, it was stated already that it can be only of case I. Since phase velocity matching is shown, the group velocities of the crossing point at frequency $2\bar{\omega}$ are obtained with Eqs. (38) and (39) for case I. Then, the factors of 2 cancel and it is shown that

$$c_{g,\mathrm{sym}}^{\mathrm{I}} = c_{g,\mathrm{sym}}^{\mathrm{I},(2\omega)}, \tag{42}$$

$$c_{g,\mathrm{asym}}^{\mathrm{I}} = c_{g,\mathrm{asym}}^{\mathrm{I},(2\omega)}. \tag{43}$$

Thus, the following conclusions are made.

- If the crossing point $(\bar{\omega}, \bar{\kappa})$ is case I, then there is group velocity matching from the symmetric mode at $(\bar{\omega}, \bar{\kappa})$ to the symmetric mode at $(2\bar{\omega}, 2\bar{\kappa})$, i.e., $c_{g,\mathrm{sym}}^{\mathrm{I}} = c_{g,\mathrm{sym}}^{\mathrm{I},(2\omega)}$, as well as from the antisymmetric mode at $(\bar{\omega}, \bar{\kappa})$ to the antisymmetric mode at $(2\bar{\omega}, 2\bar{\kappa})$, i.e., $c_{g,\mathrm{asym}}^{\mathrm{I}} = c_{g,\mathrm{asym}}^{\mathrm{I},(2\omega)}$.
- If the crossing point $(\bar{\omega}, \bar{\kappa})$ is case II, then there is group velocity matching from the symmetric mode at $(\bar{\omega}, \bar{\kappa})$ to the antisymmetric mode at $(2\bar{\omega}, 2\bar{\kappa})$, i.e., $c_{g,\mathrm{sym}}^{\mathrm{II}} = c_{g,\mathrm{asym}}^{\mathrm{I},(2\omega)}$, as well as from the antisymmetric mode at $(\bar{\omega}, \bar{\kappa})$ to the symmetric mode at $(2\bar{\omega}, 2\bar{\kappa})$, i.e., $c_{g,\mathrm{asym}}^{\mathrm{II}} = c_{g,\mathrm{sym}}^{\mathrm{I},(2\omega)}$.

Table I itemizes each possible combination along with the results about the displacements at the surface, which are explored in the following.

Regarding case I crossing points, the displacements at the surface follow by substitution of Eq. (34) into Eqs. (4) and (6), setting $y=h$. For symmetric modes, one obtains

$$\tilde{u}_y^{\mathrm{I}}(h) = 0, \tag{44a}$$

$$\tilde{u}_z^{\mathrm{I}}(h) = Dh\bar{\beta}\frac{\bar{\kappa}^2 + \bar{\beta}^2}{\bar{\kappa}^2 - \bar{\beta}^2}\cos\bar{\beta}, \tag{44b}$$

where the frequency equation, Eq. (22), is applied to simplify the expression. The displacements at the surface for the antisymmetric modes take the form

$$\tilde{u}_y^{\mathrm{I}}(h) = iCh\frac{\bar{\kappa}^2 + \bar{\beta}^2}{2\bar{\kappa}}\cos\bar{\beta}, \tag{45a}$$

$$\tilde{u}_z^{\mathrm{I}}(h) = 0, \tag{45b}$$

where the frequency equation Eq. (23) is used.

Similarly, using Eq. (35) for case II crossing points yields

$$\tilde{u}_y^{\mathrm{II}}(h) = iDh\frac{\bar{\kappa}^2 + \bar{\beta}^2}{2\bar{\kappa}}\sin\bar{\beta}, \tag{46a}$$

$$\tilde{u}_z^{\mathrm{II}}(h) = 0 \tag{46b}$$

for symmetric modes, and

$$\tilde{u}_y^{\mathrm{II}}(h) = 0, \tag{47a}$$

$$\tilde{u}_z^{\mathrm{II}}(h) = -Ch\bar{\beta}\frac{\bar{\kappa}^2 + \bar{\beta}^2}{\bar{\kappa}^2 - \bar{\beta}^2}\sin\bar{\beta} \tag{47b}$$

for antisymmetric modes.

Summarizing these results with reference to Table I, either the symmetric or the antisymmetric mode at a crossing point matches phase and group velocity with the symmetric mode of the crossing point at the double frequency. Two observations deserve special mention. First, only the first two entries in Table I satisfy all the conditions required above. The other entries have either an antisymmetric secondary mode making the power flux from the primary wave zero or do not match group velocity. Second, for all the relevant pairs, the normal displacements at the surface are identically zero.

B. Symmetric modes at the longitudinal velocity

An investigation of symmetric Lamb modes at the longitudinal phase velocity c_L with regard to the out-of-plane displacement at the free surface and group velocity was pre-

sented by Pilarski *et al.*[14] They provide frequency-thickness products, where phase velocity equals longitudinal velocity. Then, they prove that the normal displacement at the surface vanishes and that all modes at these points have the same group velocity, which depends on the linear material properties only. This section considers these results in terms of phase and group velocity matching.

Using the condition $c_{\mathrm{ph}}=c_L$, one obtains

$$\bar{\alpha}=0, \quad \bar{\beta}=n\pi, \quad n\in\mathbb{N}^+ \tag{48}$$

to satisfy the frequency relation. The corresponding frequencies

$$\bar{\omega}=\frac{n\pi c_T}{\sqrt{1-(c_T/c_L)^2}}, \quad n\in\mathbb{N}^+ \tag{49}$$

are obtained from Eqs. (5) and (48). Assuming phase velocity matching yields

$$\bar{\alpha}^{(2\omega)}=0, \quad \bar{\beta}^{(2\omega)}=2n\pi, \quad n\in\mathbb{N}^+, \tag{50}$$

which satisfies Eq. (48). Thus, there is phase velocity matching from each symmetric mode at the frequencies described in Eq. (49) to another symmetric mode at the double frequency both having the longitudinal phase velocity.

Substitution of Eq. (48) into the relation for the group velocity Eq. (24) results in

$$c_g=\frac{\bar{\kappa}(\bar{\kappa}^2-\bar{\beta}^2)^2+8\bar{\beta}^2\bar{\kappa}^3}{(\bar{\omega}/c_T^2)(\bar{\kappa}^2-\bar{\beta}^2)^2+8\bar{\beta}^2\bar{\kappa}^2(\bar{\omega}/c_L^2)}, \tag{51}$$

where the limit $\sin(\bar{\alpha})\approx\bar{\alpha}$ is used, since $\bar{\alpha}$ is very small. This is simplified as

$$c_g=\frac{c_L c_T^2(c_L^4+4c_L^2c_T^2-4c_T^4)}{12c_L^2c_T^4-4c_L^4c_T^2+c_L^6-8c_T^6} \tag{52}$$

and thus depends only on the material's properties. Consequently, the group velocity is constant for all symmetric modes at the longitudinal phase velocity. This means, for each phase velocity matching pair, group velocity matching is fulfilled as well. Note that Pilarski *et al.*[14] obtained another value for the group velocity. Confidence in the value presented here is gained by comparison to numerical results from the software DISPERSE.[16]

The displacement field in Eq. (4) yields

$$\tilde{u}_y(h)=0, \tag{53}$$

if the conditions of Eq. (48) are satisfied, i.e., the normal displacement at the surface is zero. Using the frequency Eq. (22), the in-plane displacement at the surface becomes

$$\tilde{u}_z(h)=Dh\bar{\beta}\frac{\bar{\kappa}^2+\bar{\beta}^2}{\bar{\kappa}^2-\bar{\beta}^2}\cos\bar{\beta}, \tag{54}$$

which is nonzero.

In summary, each symmetric mode at the longitudinal phase velocity shows phase and group velocity matching to another symmetric mode at the double frequency. The respective frequencies and the common group velocity are given above. As is the case for crossing points, the out-of-plane displacement at the surface is zero, while the in-plane displacement at the surface is nonzero.

C. Nonzero order modes near cutoff frequencies

Graff[8] provided a concise introduction to cutoff frequencies, which are obtained for the low wave number limit $\bar{\kappa}\to 0$. This section relates Graff's results to phase and group velocity matching.

In the low wave number limit $\bar{\kappa}\to 0$,

$$\bar{\alpha}\to\frac{\bar{\omega}}{c_L}, \quad \bar{\beta}\to\frac{\bar{\omega}}{c_T}, \tag{55}$$

hold, which leads to the conditions

$$\text{case SI:} \quad \bar{\alpha}\to\frac{(2n-1)\pi}{2}, \quad n\in\mathbb{N}^+ \tag{56a}$$

or

$$\text{case SII:} \quad \bar{\beta}\to n\pi, \quad n\in\mathbb{N}^+, \tag{56b}$$

for symmetric modes, and

$$\text{case AI:} \quad \bar{\alpha}\to n\pi, \quad n\in\mathbb{N}^+ \tag{56c}$$

or

$$\text{case AII:} \quad \bar{\beta}\to\frac{(2n-1)\pi}{2}, \quad n\in\mathbb{N}^+, \tag{56d}$$

for antisymmetric modes. From Eqs. (55) and (56), the respective cutoff frequencies are obtained as

$$\text{case SI:} \quad \bar{\omega}\to\frac{(2n-1)\pi}{2}c_L, \quad n\in\mathbb{N}^+, \tag{57a}$$

$$\text{case SII:} \quad \bar{\omega}\to n\pi c_T, \quad n\in\mathbb{N}^+, \tag{57b}$$

$$\text{case AI:} \quad \bar{\omega}\to n\pi c_L, \quad n\in\mathbb{N}^+, \tag{57c}$$

$$\text{case AII:} \quad \bar{\omega}\to\frac{(2n-1)\pi}{2}c_T, \quad n\in\mathbb{N}^+. \tag{57d}$$

To show phase velocity matching for a case SI mode in the limit $\bar{\kappa}\to 0$, the phase velocity matching conditions are applied to Eq. (56a) to obtain

$$\bar{\alpha}_{\mathrm{SI}}^{(2\omega)}=(2n-1)\pi\in\text{case AI}, \tag{58a}$$

where the subindex indicates the type of the mode at frequency $\bar{\omega}$. This means that there is phase velocity matching from every case SI mode to the case AI mode at the double frequency. Similarly, the phase velocity matching conditions for the other cases

$$\bar{\beta}_{\mathrm{SII}}^{(2\omega)}=2n\pi\in\text{case SII}, \tag{58b}$$

$$\bar{\alpha}_{\mathrm{AI}}^{(2\omega)}=2n\pi\in\text{case AI}, \tag{58c}$$

$$\bar{\beta}_{\mathrm{AII}}^{(2\omega)}=(2n-1)\pi\in\text{case SII} \tag{58d}$$

are obtained. In other words, in the limit $\bar{\kappa}\to 0$ there is phase

TABLE II. Phase velocity matching mode pairs at cutoff frequencies.

From mode at $\bar{\omega}$				To mode at $2\bar{\omega}$			
Case	$\bar{\alpha}$, $\bar{\beta}$	$\tilde{u}_y(h)$	$\tilde{u}_z(h)$	Case	$\bar{\alpha}$, $\bar{\beta}$	$\tilde{u}_y(h)$	$\tilde{u}_z(h)$
SII	$\bar{\beta}=n\pi$	0	$\neq 0$	SII	$\bar{\beta}=2n\pi$	0	$\neq 0$
AII	$\bar{\beta}=\frac{(2n-1)\pi}{2}$	0	$\neq 0$	SII	$\bar{\beta}=(2n-1)\pi$	0	$\neq 0$
SI	$\bar{\alpha}=\frac{(2n-1)\pi}{2}$	$\neq 0$	0	AI	$\bar{\alpha}=(2n+1)\pi$	$\neq 0$	0
AI	$\bar{\alpha}=n\pi$	$\neq 0$	0	AI	$\bar{\alpha}=2n\pi$	$\neq 0$	0

velocity matching:

- from every case SI symmetric mode to a case AI antisymmetric mode,
- from every case SII symmetric mode to a case SII symmetric mode,
- from every case AI antisymmetric mode to a case AI antisymmetric mode, and
- from every case AII antisymmetric mode to a case SII symmetric mode.

Note that $c_{\mathrm{ph}}\to\infty$ as $\bar{\kappa}\to 0$, and thus, phase velocity matching in this limiting case means that both phase velocities of the mode pair approach infinity.

The group velocities for all the modes described above converge to zero, i.e.,

$$c_g^i \to 0, \quad i=\mathrm{SI,SII,AI,AII} \tag{59}$$

as $\bar{\kappa}\to 0$, which is observed by Eqs. (24) and (25). Using the relations for the cutoff frequencies above, all the terms in the nominator tend to zero, while there is always a term in the denominator that does not vanish. Hence, each phase velocity matching pair shows group velocity matching with the group velocity tending to zero.

Graff's[8] results are presented for the surface displacements. The displacements of symmetric modes become

$$\tilde{u}_y(y) \to -\frac{A}{h}\bar{\alpha}\sin\bar{\alpha}\frac{y}{h}, \tag{60a}$$

$$\tilde{u}_z(y) \to -\frac{D}{h}\bar{\beta}\cos\bar{\beta}\frac{y}{h}, \tag{60b}$$

as $\bar{\kappa}\to 0$, where A is another arbitrary complex constant. For case I, the boundary conditions require $D=0$, thus

$$\tilde{u}_y^{\mathrm{SI}}(h) \to -\frac{A}{h}\bar{\alpha}\sin\bar{\alpha}, \quad \tilde{u}_z^{\mathrm{SI}}(h)\to 0 \tag{61}$$

with $\bar{\alpha}\to(2n-1)\pi/2$. For case SII, on the other hand, $A=0$ is required, resulting in

$$\tilde{u}_y^{\mathrm{SII}}(h) \to 0, \quad \tilde{u}_z^{\mathrm{SII}}(h) \to -\frac{D}{h}\bar{\beta}\cos\bar{\beta} \tag{62}$$

with $\bar{\beta}\to n\pi$.

Regarding antisymmetric modes, the displacement field reduces to

$$\tilde{u}_y(y) \to \frac{B}{h}\bar{\alpha}\cos\bar{\alpha}\frac{y}{h}, \tag{63a}$$

$$\tilde{u}_z(y) \to \frac{C}{h}\bar{\beta}\sin\bar{\beta}\frac{y}{h} \tag{63b}$$

with the complex constant B. For case AI, the boundary conditions yield $C=0$, or

$$\tilde{u}_y^{\mathrm{AI}}(h) \to \frac{B}{h}\bar{\alpha}\cos\bar{\alpha}, \quad \tilde{u}_z^{\mathrm{AI}}(h)\to 0 \tag{64}$$

with $\bar{\alpha}\to n\pi$, while case AII requires $B=0$, and thus

$$\tilde{u}_y^{\mathrm{AII}}(h) \to 0, \quad \tilde{u}_z^{\mathrm{AII}}(h) \to \frac{C}{h}\bar{\beta}\sin\bar{\beta}, \tag{65}$$

where $\bar{\beta}\to(2n-1)\pi/2$.

Table II shows all the possible combinations with their displacements at the surface. Again, only symmetric modes at double frequencies are useful for second harmonic generation, i.e., the first two entries in the table. One observes—as in Secs. VI A and VI B—that the out-of-plane displacement at the surface for these modes is zero, while the in-plane component is nonzero. For $\bar{\kappa}=0$, the group velocity is zero, meaning that no energy is carried and the wave does not propagate. For this reason, these modes are practically relevant only in the approximation where $\bar{\kappa}$ is small, but nonzero. Then, phase velocity matching holds approximately, and the group velocity and the normal displacement at the surface is small, but nonzero.

D. Nonzero order modes with high wave number

For high wave numbers, i.e., $\bar{\kappa}\to\infty$, nonzero order modes show a nondispersive behavior. It will be shown that both the phase and the group velocity converge to the shear wave speed c_T for all nonzero order modes, and thus satisfy approximately the matching conditions.

In this section, the region $c_T<c_{\mathrm{ph}}<c_L$ is considered. It follows that $\bar{\alpha}=\bar{\alpha}'i$, where

$$\bar{\alpha}' = \sqrt{\bar{\kappa}^2-\left(\frac{\bar{\omega}}{c_L}\right)^2}, \tag{66}$$

and thus, the frequency equations are

$$\Phi_{\mathrm{sym}}(\bar{\omega},\bar{\kappa}) = \sin\bar{\beta}\left[1-\left(\frac{\bar{\beta}}{\bar{\kappa}}\right)^2\right]^2 - 4\tanh\bar{\alpha}'\cos\bar{\beta}\,\frac{\bar{\alpha}'\bar{\beta}}{\bar{\kappa}^2} = 0 \tag{67}$$

and

$$\Phi_{\mathrm{asym}}(\bar{\omega},\bar{\kappa}) = \cos\bar{\beta}\left[1-\left(\frac{\bar{\beta}}{\bar{\kappa}}\right)^2\right]^2 + 4\coth\bar{\alpha}'\sin\bar{\beta}\,\frac{\bar{\alpha}'\bar{\beta}}{\bar{\kappa}^2} = 0. \tag{68}$$

In the high wave number limit $\bar{\kappa}\to\infty$, requiring

$$\bar{\beta}\to n\pi, \quad n\in\mathbb{N}^+ \tag{69}$$

satisfies Eq. (67) for symmetric modes. Similarly, Eq. (68) for antisymmetric modes holds for

$$\bar{\beta}\to\frac{(2n-1)\pi}{2}, \quad n\in\mathbb{N}^+. \tag{70}$$

In these cases, since

$$\frac{\bar{\beta}}{\bar{\kappa}} = \sqrt{\left(\frac{c_{\mathrm{ph}}}{c_T}\right)^2 - 1}\to 0, \tag{71}$$

one concludes $c_{\mathrm{ph}}\to c_T$, and

$$\bar{\alpha}' = \bar{\kappa}\sqrt{1-\left(\frac{c_{\mathrm{ph}}}{c_L}\right)^2}\to\bar{\kappa}\gamma\to\infty, \tag{72}$$

where $\gamma=\sqrt{1-(c_T/c_L)^2}$. That is, the phase velocity of all the nonzero order modes converges to the shear velocity for $\bar{\kappa}\to\infty$. Furthermore, since $\bar{\omega}\to c_T\bar{\kappa}\to\infty$, the frequency increases with wave number.

Since all the nonzero order modes converge to the same phase velocity, there is phase velocity matching from each of these modes to every nonzero order mode in the high wave number limit $\bar{\kappa}\to\infty$. This also implies that the modes show a nondispersive behavior, meaning that $\partial c_{\mathrm{ph}}/\partial\bar{\omega}=0$. From Eq. (28),

$$c_g\to c_{\mathrm{ph}}\to c_T \tag{73}$$

follows, i.e., the group velocities of all the nonzero order modes converge to the shear velocity. Thus, group velocity matching from each to every nonzero order mode is concluded for the limit $\bar{\kappa}\to\infty$.

For the subsequent investigation of the displacements, the limits

$$\frac{(\bar{\kappa}^2-\bar{\beta}^2)}{\bar{\kappa}} = \bar{\kappa}\left[1-\left(\frac{\bar{\beta}}{\bar{\kappa}}\right)^2\right]\to\bar{\kappa} \tag{74}$$

and

$$\frac{(\bar{\kappa}^2-\bar{\beta}^2)}{\bar{\alpha}} = \frac{1}{\gamma}\bar{\kappa}\left[1-\left(\frac{\bar{\beta}}{\bar{\kappa}}\right)^2\right]\to\frac{\bar{\kappa}}{\gamma} \tag{75}$$

will be helpful. Another limit for symmetric modes is obtained using the frequency relation, Eq. (67),

$$\bar{\kappa}\sin\bar{\beta}\to 4\tanh\bar{\alpha}'\cos\bar{\beta}\,\frac{\bar{\alpha}'\bar{\beta}}{\bar{\kappa}}\to 4\gamma\bar{\beta}\cos\bar{\beta}<\infty, \tag{76}$$

which is used to calculate the displacements at the surface from Eq. (4),

$$\tilde{u}_y^{\mathrm{sym}}(h)\to 2iDh\gamma\bar{\beta}\cos\bar{\beta}<\infty, \tag{77a}$$

$$\tilde{u}_z^{\mathrm{sym}}(h)\to Dh\bar{\beta}\cos\bar{\beta}<\infty. \tag{77b}$$

Equation (77) suggests that the displacements at the surface are nonzero. Yet, if the depth $y^n=h/(2n)$ is considered, for example, one term in the normal displacement of Eq. (4) tends to infinity, since

$$\bar{\kappa}\sin(\bar{\beta}y^n/h)\to\bar{\kappa}\sin(\pi/2)=\bar{\kappa}\to\infty. \tag{78}$$

Thus, D has to approach zero in order to obtain a physically reasonable, finite displacement field, and the out-of-plane displacement at the surface $u_y(h)$ becomes infinitesimally small compared to the displacement $u_y(h/(2n))$, i.e.,

$$\tilde{u}_y^{\mathrm{sym}}(h)\to 0. \tag{79}$$

For the in-plane displacement $u_z(y)$, there is no depth y to make any term unbounded, so that

$$\tilde{u}_z^{\mathrm{sym}}(y)\to 0 \quad \text{for all } y \tag{80}$$

follows, i.e., the wave tends to become a pure shear wave as $\bar{\kappa}\to\infty$, propagating at the shear wave speed.

Regarding antisymmetric modes, Eqs. (68) and (70) yield the limit

$$\bar{\kappa}\cos\bar{\beta}\to -4\coth\bar{\alpha}'\sin\bar{\beta}\,\frac{\bar{\alpha}'\bar{\beta}}{\bar{\kappa}}\to -4\gamma\bar{\beta}\sin\bar{\beta}<\infty, \tag{81}$$

which is used to calculate the displacements of Eq. (6) at the surface,

$$\tilde{u}_y^{\mathrm{asym}}(h)\to -2iCh\gamma\bar{\beta}\sin\bar{\beta}<\infty, \tag{82a}$$

$$\tilde{u}_z^{\mathrm{asym}}(h)\to -Ch\bar{\beta}\sin\bar{\beta}<\infty. \tag{82b}$$

If the middle layer $y^n=0$ is considered in Eq. (6), the normal displacement tends to infinity because

$$\bar{\kappa}\cos(\bar{\beta}y^n/h)\to\bar{\kappa}\cos(0)=\bar{\kappa}\to\infty, \tag{83}$$

while there is no y that makes the in-plane displacement unbounded. Hence, with the same argument as above,

$$\tilde{u}_y^{\mathrm{asym}}(h)\to 0 \tag{84}$$

and

$$\tilde{u}_z^{\mathrm{asym}}(y)\to 0 \quad \text{for all } y. \tag{85}$$

Thus, as $\bar{\kappa}\to\infty$, both symmetric and antisymmetric modes tend to become pure shear waves at the shear velocity with zero displacements at the surface.

In summary, as $\bar{\kappa}\to\infty$ in the region $c_T<c_{\mathrm{ph}}<c_L$, it is shown that all nonzero order modes approach the shear ve-

locity c_T in both the phase and the group velocity. Hence, phase and group velocity matching is concluded from each to every mode in the high wave number limit. Furthermore, the out-of-plane displacement at the surface and the in-plane displacement over the whole cross section converge to zero, so that the motion becomes pure shear. From a practical perspective, the results may be applied approximately, i.e., as $\bar{\kappa}$ becomes large but not infinity. Then, depending on the wave number and the approximation tolerance applied, the results hold for a certain number of modes.

E. Fundamental modes with high wave number (quasi-Rayleigh surface wave)

In the region $c_{\mathrm{ph}}<c_T<c_L$ for $\bar{\kappa}\to\infty$, the fundamental modes take the form of a Rayleigh surface wave, called a quasi-Rayleigh wave for plates. The additional term *quasi* indicates that this is not the original Rayleigh wave—as defined for a semi-infinite half-space—but the Lamb modes that behave like a Rayleigh wave in the high frequency domain. As $\bar{\kappa}$ increases, the wavelength becomes much smaller than the plate's thickness, so that the plate appears approximately as a semi-infinite half-space.

The condition $c_{\mathrm{ph}}<c_T$ implies that $\bar{\alpha}$ and $\bar{\beta}$ are complex and written as $\bar{\alpha}=i\bar{\alpha}'$ and $\bar{\beta}=i\bar{\beta}'$, where $\bar{\alpha}'$ as in Eq. (66) and

$$\bar{\beta}' = \sqrt{\bar{\kappa}^2 - \left(\frac{\bar{\omega}}{c_T}\right)^2}. \tag{86}$$

The frequency equations (22) and (23) reduce to the Rayleigh wave equation

$$(\bar{\kappa}^2 + \bar{\beta}'^2)^2 - 4\bar{\alpha}'\bar{\beta}'\bar{\kappa}^2 = 0, \tag{87}$$

whose solution is the Rayleigh wave speed c_R with the property $c_R<c_T$. Hence, the limits

$$\bar{\alpha}' = \bar{\kappa}\sqrt{1-\left(\frac{c_R}{c_L}\right)^2} \to \bar{\kappa}\gamma_\alpha \to \infty, \tag{88}$$

$$\bar{\beta}' = \bar{\kappa}\sqrt{1-\left(\frac{c_R}{c_T}\right)^2} \to \bar{\kappa}\gamma_\beta \to \infty \tag{89}$$

are concluded, where $\gamma_\alpha=\sqrt{1-(c_R/c_L)^2}$ and $\gamma_\beta=\sqrt{1-(c_R/c_T)^2}$.

Since both fundamental modes $A0$ and $S0$ converge to the Rayleigh wave speed in the high wave number limit $\bar{\kappa}\to\infty$, there is phase velocity matching from each fundamental mode to itself and to the other one. As in Sec. VI D, group velocity equals phase velocity, i.e.,

$$c_g \to c_{\mathrm{ph}} \to c_R \tag{90}$$

due to the nondispersive behavior and Eq. (28). Hence, group velocity matching for the fundamental modes is concluded.

Substituting the limits obtained above in the displacement fields, Eqs. (4) and (6) result in

$$\tilde{u}_y^{S0}(y) = \frac{D\bar{\kappa}}{h}\left(\frac{(1+\gamma_\beta^2)\sinh\bar{\beta}'}{2\sinh\bar{\alpha}'}\sinh\left(\bar{\alpha}'\frac{y}{h}\right) - \sinh\left(\bar{\beta}'\frac{y}{h}\right)\right), \tag{91a}$$

$$\tilde{u}_z^{S0}(y) = \frac{iD\bar{\kappa}}{h}\left(\frac{(1+\gamma_\beta^2)\sinh\bar{\beta}'}{2\gamma_\alpha\sinh\bar{\alpha}'}\cosh\left(\bar{\alpha}'\frac{y}{h}\right) - \gamma_\beta\cosh\left(\bar{\beta}'\frac{y}{h}\right)\right) \tag{91b}$$

for the symmetric fundamental mode $S0$, and

$$\tilde{u}_y^{A0}(y) = \frac{iC\bar{\kappa}}{h}\left(-\frac{(1+\gamma_\beta^2)\cosh\bar{\beta}'}{2\cosh\bar{\alpha}'}\cosh\left(\bar{\alpha}'\frac{y}{h}\right) + \cosh\left(\bar{\beta}'\frac{y}{h}\right)\right), \tag{92a}$$

$$\tilde{u}_z^{A0}(y) = \frac{C\bar{\kappa}}{h}\left(\frac{(1+\gamma_\beta^2)\cosh\bar{\beta}'}{2\gamma_\alpha\cosh\bar{\alpha}'}\sinh\left(\bar{\alpha}'\frac{y}{h}\right) - \gamma_\beta\sinh\left(\bar{\beta}'\frac{y}{h}\right)\right) \tag{92b}$$

for the antisymmetric fundamental mode $A0$. These equations show—according to the theory of Rayleigh waves—that the energy is concentrated at the surface and that displacements vanish exponentially with depth. As $\bar{\alpha}'$ and $\bar{\beta}'$ become large, the $\sinh(\cdot)$ and $\cosh(\cdot)$ terms grow with a faster exponential rate as y approaches h. In the very limit $\bar{\alpha}', \bar{\beta}'\to\infty$, the displacement is concentrated entirely in an infinitesimally small layer beneath the surface. Therefore, large out-of-plane and in-plane displacements are observed at the plate's surface.

In summary, for large wave numbers and frequencies, both the phase and the group velocity of the fundamental modes $S0$ and $A0$ converge to the Rayleigh surface wave speed $c_R<c_T$. Due to its nondispersive behavior, both phase and group velocity matching are concluded. The displacements at the surface are large as compared to the inner part of the plate, since energy is concentrated in a thin layer beneath the surface.

VII. CONCLUSION

This research considers the conditions for the second harmonic generation of Lamb waves using these results to determine five different types of matching pairs of Lamb modes with internal resonance. These matching mode pairs all satisfy the conditions of nonzero power flux to the second harmonic wave, phase velocity matching, and group velocity matching. The first condition is shown to be satisfied if symmetric second harmonic modes are considered. For the velocity matching conditions, two mode types match phase and group velocity exactly (crossing points and symmetric modes at the longitudinal velocity), while three mode types match

approximately (modes near cutoff frequencies, nonzero order modes for high wave numbers, and quasi-Rayleigh wave). The analysis of these matching mode pairs provides critical information for their experimental generation and detection such as excitation frequencies, and related quantities such as phase and group velocity. In addition, it is shown that all these mode pairs (except for the quasi-Rayleigh pair) that satisfy internally resonant second harmonic generation also display zero out-of-plane displacements at the surface.

These results provide a suite of potential mode combinations that can be used to experimentally measure a second harmonic amplitude that is linearly increasing with propagation distance, potentially with a higher signal-to-noise ratio. These measured second harmonic amplitudes enable the direct characterization of a material's nonlinear elastic components and the associated damage state.

ACKNOWLEDGMENTS

This work was partially supported by the National Science Foundation under Contract No. CMMI-0653883 and the Air Force Office of Scientific Research under Contract No. FA9550-08-1-0241. The Deutscher Akademischer Austauschdienst (DAAD) provided partial support to Martin F. Müller.

APPENDIX: EXPANSION OF FORCING TERM

$$\bar{S}_{yy} = \left(\frac{3\lambda}{2} + 3\mu + \bar{A} + 3\bar{B} + \bar{C}\right)\frac{\partial u_y}{\partial y}\frac{\partial u_y}{\partial y} + \left(\frac{\lambda}{2} + \mu + \frac{\bar{A}}{4} + \frac{\bar{B}}{2}\right)\left(\frac{\partial u_y}{\partial z}\frac{\partial u_y}{\partial z} + \frac{\partial u_z}{\partial y}\frac{\partial u_z}{\partial y}\right) + \left(\frac{\lambda}{2} + \bar{B} + \bar{C}\right)\frac{\partial u_z}{\partial z}\frac{\partial u_z}{\partial z} + (\lambda + 2\bar{B} + 2\bar{C})\frac{\partial u_y}{\partial y}\frac{\partial u_z}{\partial z} + \left(\mu + \frac{\bar{A}}{2} + \bar{B}\right)\frac{\partial u_y}{\partial z}\frac{\partial u_z}{\partial y}, \tag{A1}$$

$$\bar{S}_{zz} = \left(\frac{3\lambda}{2} + 3\mu + \bar{A} + 3\bar{B} + \bar{C}\right)\frac{\partial u_z}{\partial z}\frac{\partial u_z}{\partial z} + \left(\frac{\lambda}{2} + \mu + \frac{\bar{A}}{4} + \frac{\bar{B}}{2}\right)\left(\frac{\partial u_y}{\partial z}\frac{\partial u_y}{\partial z} + \frac{\partial u_z}{\partial y}\frac{\partial u_z}{\partial y}\right) + \left(\frac{\lambda}{2} + \bar{B} + \bar{C}\right)\frac{\partial u_y}{\partial y}\frac{\partial u_y}{\partial y} + (\lambda + 2\bar{B} + 2\bar{C})\frac{\partial u_y}{\partial y}\frac{\partial u_z}{\partial z} + \left(\mu + \frac{\bar{A}}{2} + \bar{B}\right)\frac{\partial u_y}{\partial z}\frac{\partial u_z}{\partial y}, \tag{A2}$$

$$\bar{S}_{yz} = \left(\lambda + 2\mu + \frac{\bar{A}}{2} + \bar{B}\right)\left(\frac{\partial u_y}{\partial y}\frac{\partial u_z}{\partial y} + \frac{\partial u_z}{\partial z}\frac{\partial u_z}{\partial y}\right) + \left(\mu + \frac{\bar{A}}{2} + \bar{B}\right)\left(\frac{\partial u_y}{\partial y}\frac{\partial u_y}{\partial z} + \frac{\partial u_z}{\partial z}\frac{\partial u_y}{\partial z}\right), \tag{A3}$$

$$\bar{S}_{zy} = \left(\lambda + 2\mu + \frac{\bar{A}}{2} + \bar{B}\right)\left(\frac{\partial u_y}{\partial y}\frac{\partial u_y}{\partial z} + \frac{\partial u_z}{\partial z}\frac{\partial u_y}{\partial z}\right) + \left(\mu + \frac{\bar{A}}{2} + \bar{B}\right)\left(\frac{\partial u_y}{\partial y}\frac{\partial u_z}{\partial y} + \frac{\partial u_z}{\partial z}\frac{\partial u_z}{\partial y}\right). \tag{A4}$$

[1] J.-Y. Kim, L. J. Jacobs, J. Qu, and J. W. Littles, "Experimental characterization of fatigue damage in a nickel-base superalloy using nonlinear ultrasonic waves," J. Acoust. Soc. Am. **120**, 1266–1273 (2006).
[2] J. Herrmann, J.-Y. Kim, L. J. Jacobs, J. Qu, J. W. Littles, and M. F. Savage, "Assessment of material damage in a nickel-base superalloy using nonlinear Rayleigh surface waves," J. Appl. Phys. **99**, 124913 (2006).
[3] C. Pruell, J.-Y. Kim, J. Qu, and L. J. Jacobs, "Evaluation of plasticity driven material damage using Lamb waves," Appl. Phys. Lett. **91**, 231911 (2007).
[4] C. Pruell, J.-Y. Kim, J. Qu, and L. J. Jacobs, "Evaluation of fatigue damage using nonlinear guided waves," Smart Mater. Struct. **18**, 035003 (2009).
[5] W. J. de Lima and M. F. Hamilton, "Finite-amplitude waves in isotropic elastic plates," J. Sound Vib. **265**, 819–839 (2003).
[6] M. Deng, "Analysis of second-harmonic generation of Lamb modes using a modal analysis approach," J. Appl. Phys. **94**, 4152–4159 (2003).
[7] A. Srivastava and F. L. di Scalea, "On the existence of antisymmetric or symmetric Lamb waves at nonlinear higher harmonics," J. Sound Vib. **323**, 932–943 (2009).
[8] K. F. Graff, *Wave Motion in Elastic Solids* (Oxford University Press, London, 1975).
[9] J. D. Achenbach, *Wave Propagation in Elastic Solids* (Elsevier Science B.V, Amsterdam, 1975).
[10] L. D. Landau and E. M. Lifshitz, *Theory of Elasticity* (Pergamon, New York, 1986).
[11] M. Deng, "Cumulative second-harmonic generation of Lamb-mode propagation in a solid plate," J. Appl. Phys. **85**, 3051–3058 (1999).
[12] M. Deng, P. Wang, and X. Lv, "Experimental observation of cumulative second-harmonic generation of Lamb-wave propagation in an elastic plate," J. Phys. D: Appl. Phys. **38**, 344–353 (2005).
[13] T.-H. Lee, I.-H. Choi, and K.-Y. Jhang, "The nonlinearity of guided wave in an elastic plate," Mod. Phys. Lett. B **22**, 1135–1140 (2008).
[14] A. Pilarski, J. J. Ditri, and J. L. Rose, "Remarks on symmetric Lamb waves with dominant longitudinal displacements," J. Acoust. Soc. Am. **93**, 2228–2230 (1993).
[15] J. L. Rose, *Ultrasonic Waves in Solid Media* (Cambridge University Press, Cambridge, 1999).
[16] B. Pavlakovic and M. Lowe, DISPERSE, User's Manual Version 2.0.11, Software Version 2.0.15e, Imperial College, London, England (2001).